Energy Storage Materials 22 (2019) 96–104

Contents lists available at ScienceDirect

Energy Storage Materials

journal homepage: www.elsevier.com/locate/ensm

Kinetic surface control for improved magnesium-electrolyte interfaces for magnesium ion batteries

Bin Li [a,b,1], Robert Masse [a,1], Chaofeng Liu [a], Yang Hu [a], Weishan Li [c], Guoqing Zhang [b], Guozhong Cao [a,*]

[a] Department of Materials Science and Engineering, University of Washington, Seattle, WA, 98195, USA
[b] School of Materials and Energy, Guangdong University of Technology, Guangzhou, 510006, PR China
[c] School of Chemistry and Environment, Key Laboratory of Electrochemical Technology on Energy Storage and Power Generation of Guangdong Higher Education Institutes, Engineering Research Center of Materials and Technology for Electrochemical Energy Storage (Ministry of Education), South China Normal University, Guangzhou, 510006, China

ARTICLE INFO

Keywords:
Magnesium ion battery
Magnesium metal
Electrolyte
Interface
Magnesium fluoride

ABSTRACT

Magnesium (Mg) metal is a compelling battery anode material for Mg ion batteries because of its high volumetric energy density, good operational safety and abundance. The metal promises extremely high energy density and much safer compared to Li metal due to less dendrite growth. However, most conventional battery electrolytes react with Mg to form blocking layers. Much attention has been dedicated to synthesizing electrolytes that are thermodynamically stable with respect to Mg metal. Here we report a new approach to improving the (electro) chemical compatibility of the Mg-electrolyte interface by exerting kinetic control instead. A chemically inert magnesium fluoride (MgF_2) layer is formed through controlled reaction of Mg surface with hydrofluoric acid. The tailored surface layer improves the voltage stability, Coulombic efficiency, and cycling performance of full-cell Mg ion batteries compared to cells using bare Mg metal as an anode. Remarkably, unlike almost all other Mg surface films, the MgF_2 passivating layer not only suppresses side reactions with the electrolyte but also allows for Mg^{2+} transport between the electrode and electrolyte. This result reinforces the importance of controlling Mg surface chemistry for the successful development of high-energy magnesium ion batteries.

1. Introduction

With increasing demands for portable energy storage in electronics and electric vehicles, better batteries beyond current Li-ion batteries (LIBs) are a necessity. Rechargeable magnesium (Mg) ion batteries have emerged as an attractive alternative because of the unique advantages of Mg metal. These include as large specific capacity (3833 mAh cm^{-3} and 2205 mAh g^{-1}), easy handling, high abundance, and theoretically smooth electrodeposition on Mg metal [1–5].

Despite these compelling features, the Mg metal anodes are incompatible with many electrolytes [6]. Conventional electrolytes (for example, $Mg(BF_4)_2$, $Mg(ClO_4)_2$ or $Mg(PF_6)_2$ dissolved in organic solvents) are reduced by Mg to form insoluble passivation layers on the Mg metal surface [7,8]. Unlike the solid-electrolyte interphase (SEI) layer in LIBs, the Mg passivation layer blocks transport of both ions and electrons and makes the electrochemical deposition/stripping of Mg impossible [3,9]. On the other hand, the electrolytes that allow for reversible plating and stripping of Mg at the metal anode surface (Grignard reagents and other organohaloaluminate electrolytes) suffer from poor stability at voltages beyond ~2 V (*vs.* Mg/Mg^{2+}) [1,10–14]. Most recently, a class of electrolytes with stabilities beyond 3 V (*vs.* Mg/Mg^{2+}) and reversible Mg plating/stripping have been developed, but require complicated organic syntheses [15–18].

The anode-electrolyte interface governs the performance and longevity of the cell and has been the subject of many studies [7,19–24]. As early as 2003, it was believed that a stable "passivation layer" develops on fresh magnesium metal foil submerged in solutions of tetrahydrofuran (THF) and $Mg(AlEtBuCl_2)_2$ - an electrolyte that supports Mg stripping and plating, and it was suggested the layer contained physically adsorbed molecules rather than ionic species on the Mg surface [25]. More recently, the influence of adsorbed Mg_x-Cl_y species has been identified as a key factor that benefits reversible plating of magnesium

* Corresponding author.
E-mail address: gzcao@uw.edu (G. Cao).
[1] equal contribution and co-first authors.

https://doi.org/10.1016/j.ensm.2019.06.035
Received 15 February 2019; Received in revised form 17 June 2019; Accepted 29 June 2019
Available online 2 July 2019

because of their preferential adsorption and low energies required to remove chloride ligands from Mg^{2+} [26,27]. In addition, adding $MgCl_2$ greatly improves the performance of electrolytes by shifting the equilibrium concentration of the Mg_x-Cl_y species and greatly reducing the overpotential for stripping and plating [28].

However, this strategy is limited for two reasons. The volatile solvent with a low boiling point (66 °C for THF) leads to additional safety considerations, while chloride-containing electrolytes are corrosive towards common battery components like stainless steels [3,29,30]. While commercially practical electrolytes have not yet been realized, good progress has been made to increase the thermodynamic stability of the electrolyte, especially in the last decade [5,31,32]. Notably, a recent trend to reduce chlorine content in electrolytes has enabled the discovery of noncorrosive electrolytes with good conductivity (>1 mS cm^{-1}), efficient Mg dissolution/deposition (>98% Coulombic efficiency) and anodic stability well beyond 3 V (*vs.* Mg/Mg^{2+}) [17,33,34]. However, these novel electrolytes often require complicated procedures and toxic chemicals that are best left to synthetic organometallic chemists [35].

Here we report an alternative path forward using kinetic control of the anode-electrolyte interface. By passivating the Mg metal surface with fluorine, we develop what is to our knowledge the first Mg^{2+}-conductive passivating layer formed on Mg metal. This strategy avoids the complication of time consuming syntheses and provides a possible avenue toward non-corrosive electrolytes compatible with stainless steel and other common battery components, while simultaneously allowing for transport of Mg^{2+}. This approach, with one chemical in one step, is much simpler and more straightforward than that in LIBs. In LIBs, the reduction products that form the SEI layer on the surface of the electrode materials has enormous influence on the electrochemical behavior of the batteries [36–38]. The morphology and structure (thickness, component, and size) of the SEI films can be turned using electrolyte additives like vinylene carbonate [39,40], fluoroethylene carbonate [41], vinyl ethylene carbonate [42], propane sultone [43] and prop-1-ene-1,3-sultone [37,44]. These additives are preferentially decomposed to form an insoluble solid product and subsequently cover the electrode surface. These initial films inhibit further reaction with the nonaqueous liquid electrolytes. Surface modification of fluorides have also proven as an effective way to restrain the electrolyte decomposition on the surface of electrode materials and enhance the cycling stability of the LIBs [45]. It is known that inorganic fluorides such as lithium fluoride (LiF), sodium fluoride (NaF), and magnesium fluoride (MgF_2) in their bulk states are insulators and hinder the transport of ions; however, researches demonstrated that the ions transportation is possible through fluoride or fluorinated interphases. LiF or NaF artificial interphase protects the metallic anode from the side reaction and suppresses the dendrite growth [46,47]. Fluorinated interphases play an important role in electrode protection [48,49]. The interphase layers are known to be complex, often amorphous or consist of nanoparticles or a mixture of nanocrystallites and amorphous so that there are abundant grain boundaries and significant variations of local chemical composition, which might permit the ionic transportation for electrochemical reaction. MgF_2 has been widely used in various optical thin films and multilayer photonic crystals because of its low absorption, wide bandgap, high hardness and good corrosion resistance [50], and has also been used to improve the performance of LIB electrode materials. For example, MgF_2-coated lithium cobalt oxides ($LiCoO_2$) composites were developed and exhibited higher rate capability and cycling stability compared to the uncoated $LiCoO_2$ [50–52]. These reports suggested the MgF_2 layer not only reduced side reactions with electrolytes but also benefitted the migration of Li^+ between the electrolyte and the bulk $LiCoO_2$, which means the MgF_2 layer is an ionic conductor of Li^+ but an electronic insulator. Therefore, it is expected that this protective layer could inhibit the decomposition of the electrolyte in Mg ion batteries, and more importantly, allow for Mg^{2+} transport in this protective layer. In this work, we have developed a chemically inert, ionically conductive, but electronically insulating MgF_2 layer to improve the compatibility of the Mg-electrolyte interface. At the same time, its high specific surface area benefits the contact between the electrode and electrolyte. The present study shows how optimizing the surface chemistry and morphology of Mg metal surfaces are critical for Mg ion battery storage technology.

2. Results and discussion

The formation process for the MgF_2@Mg electrode is illustrated schematically in Fig. 1a (see Experimental section). To remove the oxide layer on Mg foil, Mg was first washed with diluted hydrogen chloride (HCl, 0.1 M) aqueous solution. The MgF_2 coating layer was then applied by treating the fresh Mg metal with 0.2 M hydrogen fluoride (HF) by sonication. This reaction evolves hydrogen (H_2) gas and produces the fluoride surface protection layer via a metal exchange reaction ($Mg + 2HF = MgF_2 + H_2$). No micro bubbles can be observed on the Mg surface after the ultrasonic and HF treatment, which suggests the MgF_2 layer was coated to the Mg surface and separated Mg from HF.

Using this design, the electrolyte (here, the all phenyl complex (APC) electrolyte [32]) is only in contact with the outer surface of the Mg electrode and cannot reach the inner Mg foil (Fig. 1b). The outer layer formed by MgF_2 is porous, but mechanically rigid and has a high hardness [53]. Thus, the inner Mg foil shrinks inward during the extraction, and during electrodeposition, Mg^{2+} penetrates through the passivating layer and reacts with the Mg metal. This passivation layer protects APC-based electrolytes from further decomposition on the Mg surface and favors the formation of a thin, porous passivated layer with improved interfacial transport properties. This is in contrast with the behavior of the bare Mg metal with APC. At high enough overpotentials, Mg^{2+} is extracted from regions where the bare metal has not been passivated by the electrolyte (Fig. 1c). This reaction between the metal and organohaloaluminate electrolytes is believed to be mediated by adsorbed chloride ions on the surface [27], whereas byproducts from the reduction of the electrolyte block Mg transport. When deposition takes place, Mg plating must compete with reduction of the electrolyte, leading to new growth of the surface passivation layer (Fig. 1d).

Nitrogen gas adsorption-desorption isotherms were recorded to evaluate the surface area and pore sizes. The Brunauer-Emmett-Teller (BET) derived specific surface areas of MgF_2@Mg is 6.87 $m^2 g^{-1}$, which is higher than that of fresh Mg (0.86 $m^2 g^{-1}$). The almost an order of magnitude higher surface area is largely attributable to the formation of hydrogen gas, the by-product during the deposition of MgF_2 passivation layer. The passivation layer is conformally coated on the surface of Mg electrode and provides physical barrier to prevent the direct contact between Mg and electrolyte. It is believed that a large specific surface area provides large contact area between the electrode surface and the electrolyte for more effective reaction at the interface. Additionally, the Barrett-Joyner-Halenda (BJH) pore size distribution curve obtained from the nitrogen sorption isotherms suggests that the MgF_2@Mg electrode contain broadly distributed pores, most of which are smaller than 15 nm, with an average pore diameter of ~2.5 nm (Fig. S1). The mesopore size and volume on MgF_2@Mg are advantageous for energy storage since the large pore channels permit rapid electrolyte transport. Therefore, this conformal MgF_2 layer is expected to improve the interfacial transport properties between the electrolyte and Mg electrode.

The feature of the MgF_2 coating layer on Mg metal was observed by energy dispersive X-ray spectra (EDS) mapping of the cross section for MgF_2@Mg disc as shown in Fig. 2a, fluoride element has a uniform distribution in the surface layer with <200 nm thickness on the Mg substrate, demonstrating the conformally fluoride-rich layer was formed during the HF treatment.

The compatibility of the Mg-electrolyte interface was studied with the APC electrolyte [54]. To evaluate the electrochemical properties of the MgF_2 coated Mg electrode, symmetrical Mg coin cells were assembled using the APC electrolyte and cycled at current density of 0.25 mA cm^{-2} for 75 cycles. As shown in Fig. 2b–c, the symmetrical cell based on bare Mg electrodes experienced extremely high and rapidly increased

hysteresis up to 200 mV after 60 h, then followed by an intensive increase of overpotential bumps around 65 h, which was probably caused by the passivation film derived from APC and indicating that the passivation film was unstable and high resistive. In contrast, the electrode coated with MgF_2 exhibits a lower voltage hysteresis around 25 mV indicating a smaller electrical resistance, relative to the based on the fresh Mg electrode. The small resistance might also be attributed at least in part to an order of magnitude larger specific surface area of the MgF_2 interphase layer (fresh Mg: 0.86 $m^2 g^{-1}$, MgF_2@Mg: 6.87 $m^2 g^{-1}$). After 100 cycles, the magnesium deposition/stripping process remains outstanding stable, and the flatness of the voltage versus time response seen in each cycle (Fig. 2d) suggests the magnesium deposition/stripping process is stable with no detectable degradation.

To assess the protecting ability of MgF_2 on Mg metal, cyclic voltammetry (CV) was performed at a scan rate of 0.1 mV s^{-1} between 0.01 and 0.9 V. A slow sweep rate was used in this study to gain a better fundamental understanding of the electrochemistry and electrochemical performance by avoiding the kinetic impacts and the dendritic growth of Mg. Standard coin cells (2025) were assembled using Mg foil as the negative electrode and Bi/carbon composite as the positive electrode. Bismuth (Bi) was selected in this work because of its high volumetric capacity (up to 3430 mAh cm^{-3}) and low potential for Mg alloying/de-alloying [55,56]. The Bi nanorods were synthesized via a solvothermal method using the reduction of bismuth oxide (Bi_2O_3) by ethylene glycol [57]. The morphology and structure of commercial Bi_2O_3 and the obtained Bi nanorods were characterized by scanning electron microscopy (SEM), transmission electron microscopy (TEM) and X-ray diffraction (XRD) and the results are presented in Fig. S2.

Fig. 3a–b compare the CV curves of the Mg ion batteries with anodes made of fresh Mg foil and MgF_2-coated Mg, and the reductions/oxidation peaks of the samples are listed in Table S1. The reductive current displayed at 0.01 V is attributed to Mg^{2+} insertion into Bi and consequent alloying between Mg and Bi ($2Bi + 3Mg^{2+} + 6e^- = Mg_3Bi_2$), while the oxidative peak at about 0.4 V is attributed to the de-alloying reaction [58]. These symmetric peaks indicate good reversible electrochemical insertion/extraction of Mg-ions to and from the Bi electrode. Noted that the reduction current increase with cycling in both of the samples. The increase of the reduction current is most likely associated with the wettability of electrolyte on the electrode, and also the formation of the Mg_3Bi_2 alloy. This phenomenon was also observed in different systems [59]. In the case of the cell with fresh Mg electrode, it is worth noting that large current responses were observed at above 0.5 V in the anodic scanning. The de-alloying reaction between Mg and Bi only occurs below 0.5 V, as observed in different systems and reported in literature [55,56,59], and the oxidation of APC is not expected to occur on positive electrode at this low voltage [54], so this suggests that the current responses is attributed to the decomposition of the APC electrolyte on Mg electrode surface. Anodic scanning leads to the decomposition of physically adsorbed molecular films on Mg, leaving behind a deposition layer. The layer is a kind of passivation layer but it is not sufficiently compact and stable as to protect the electrolyte from further and continued decomposition. It was observed that the alloying/de-alloying current gradually increased and the decomposition peaks still become broad during subsequent cycles (at the 2nd and 3rd cycles).

Different electrochemical behavior was recorded in the cell with MgF_2-coated Mg foil, as shown in Fig. 3b. The voltage of the alloying peak in the first cycle somewhat positively shifted to 0.18 V. It suggests that the Mg^{2+} extraction from MgF_2-coated Mg electrode is easier than the pristine electrode, which means the MgF_2 layer has higher migration and diffusion rates of Mg cation ions compares to the physically adsorbed film. In addition, the peak current of electrolyte decomposition above 0.5 V is significantly suppressed. This voltage region exhibits a low current shoulder without any discernible peak on the subsequent cycles during Mg^{2+} depositing on the Mg electrode, which suggests the MgF_2 layer can inhibit electron transfer between Mg and electrolyte and effectively protect the Mg metal surface from side reactions.

Constant current charge–discharge tests were conducted to assess the electrochemical behavior of the MgF_2-coated metal anode. Fig. 3c and d shows the charge-discharge curves of fresh Mg and MgF_2@Mg at 30 mA g^{-1} for the 1st and 2nd cycle between 0.01 and 1.0 V. It reveals that the discharge voltage drops quickly to ~0.12 V and then rises to reach a plateau at approximately 0.2 V. This feature indicates that an activation process exists, which is mostly associated with the wettability between the electrode particles and electrolyte and the growth kinetics of the Mg_3Bi_2 alloy [59]. During charging, the Mg de-insertion process in Bi starts at around 0.3 V and deposits Mg onto the Mg surface. The Mg insertion/de-insertion processes are consistent well with the CV results and suggests that Mg ions can be reversibly inserted into and extracted from the as-prepared Bi nanorods. However, at a higher de-insertion voltage, the cell with bare Mg metal displays two shoulders at around 0.5 and 0.9 V, and exhibits a Coulombic efficiency of 113% in the first cycle. These nonlinear plateaus can be assigned to electrolyte

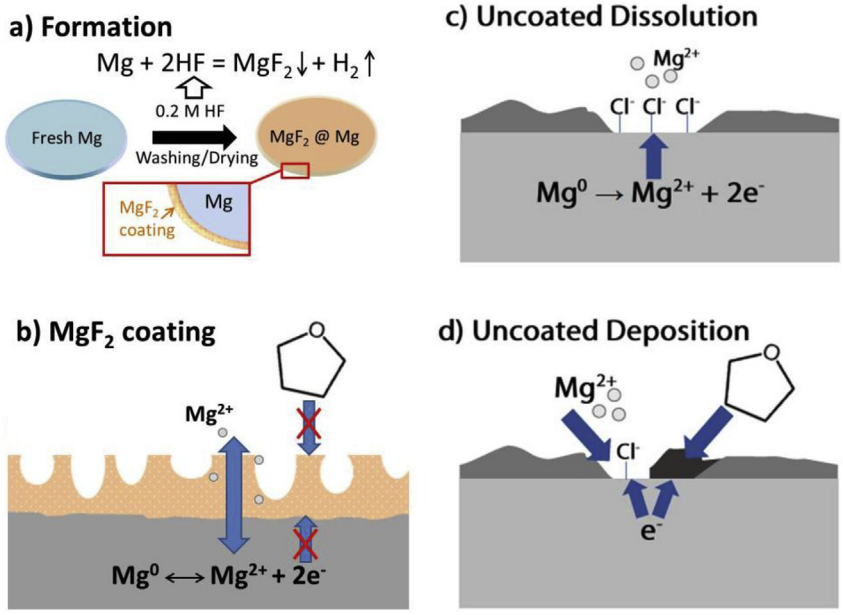

Fig. 1. (a) Schematic illustration of the formation process of the MgF_2 surface coating. (b) Schematic of the proposed operating mechanism of the MgF_2 for stripping and plating of Mg metal. (c) Compared to the MgF_2 film, Mg stripping with a conventional Mg metal anode has to proceed where the anode has not been passivated by electrolyte reduction products (dark gray). The active area is believed to contain an adsorbed layer of chloride ions. (d) Plating of the bare metal is not 100% efficient and leads to the growth of the layer electrolyte reduction products.

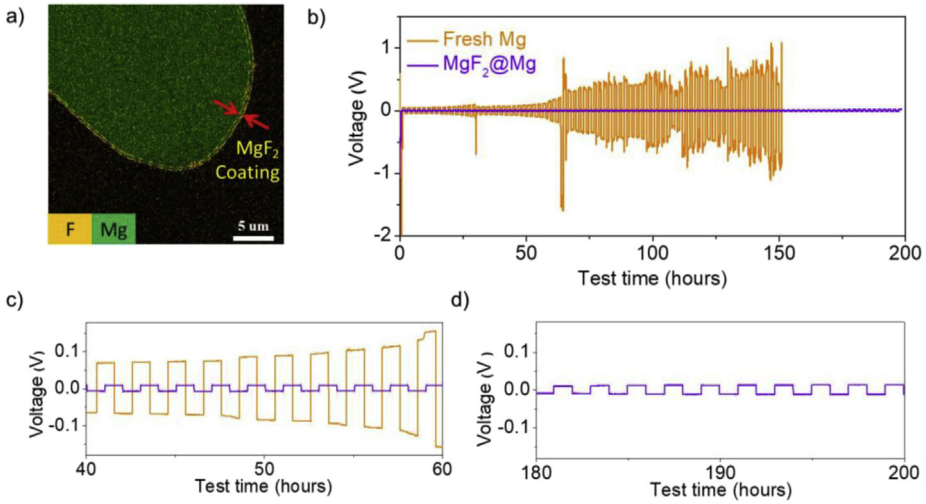

Fig. 2. (a) Cross-section EDS mapping of the as-prepared of the MgF_2@Mg electrode. (b) Voltage profiles of the symmetric cells cycling of fresh Mg and MgF_2 coated Mg at current density of 0.25 mA cm^{-2} (1 h for half cycle). (c) and (d) Magnified curves of the cycling for symmetric cells of fresh Mg (orange curve) and MgF_2@Mg (violet curve). (For interpretation of the references to color in this figure legend, the reader is referred to the Web version of this article.)

decomposition by the highly reactive Mg particles. The reaction products on the Mg surface form a passivating layer which blocks the deposition of the Mg. This instability in the voltage profile may be indicative of the unstable nature of Mg as a reference electrode [60], and suggests increased surface impedance at the anode. Therefore, more energy needs to be dedicated to pushing Mg^{2+} through whatever passivation layer may exist and less energy is committed to inserting Mg^{2+} into the Bi material. This decomposition still occurs in the charging process at higher voltage in the second cycle and presents a Coulombic efficiency of 106%. It suggests that the surface film formed on the fresh Mg surface in the first cycle cannot prevent the decomposition of the APC electrolyte, and consequently lead to the repeat consumption of the electrolyte and continuous growth of the passivating layer. For the cell using MgF_2@Mg foil, the long voltage plateau at around 0.3 V and the sharp increasing voltage starting from 0.4 V are identified during charging (Fig. 3d), which is similar to the other Bi studies [55,56]. The first charge capacity is 340 mAh g^{-1}, while the Coulombic efficiency is 90% and reaches 99% in the second cycle. Notably, the polarization of MgF_2@Mg in the second discharge curve is smaller than that of fresh Mg, indicating the dissolution of Mg^{2+} from Mg in MgF_2 layer is easier than the passivation layer derived from APC decomposition on fresh foil. These results strongly suggest that the porous MgF_2 layer prevents the decomposition of the APC electrolyte (electronically insulating) while facilitating the migration of magnesium ions (ionically conductive).

The cycling performance of fresh Mg and MgF_2@Mg are shown in Fig. 4a. The cells were charged/discharged at a current density of 30 mA g^{-1} for initial two cycles, followed by cycling at a current density of 120 mA g^{-1} in the voltage range of 0.01-1.0 V. The charge capacity of the

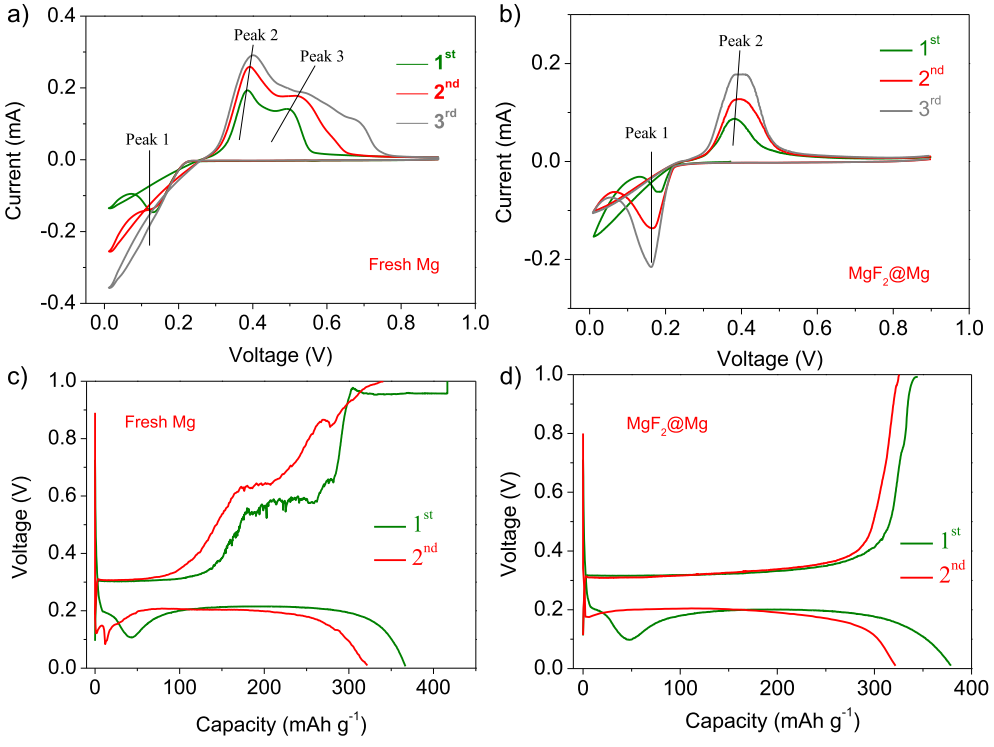

Fig. 3. Cyclic voltammograms using Bi nanorods as positive electrode and different magnesium foils as negative electrodes: (a) Fresh Mg foil and (b) MgF_2@Mg foil; Scan rate: 0.1 mV s^{-1}. After coating the metal with MgF_2, the close voltage difference of the first cycle, ~0.2 V, between ions-insertion and extraction processes seems to show fast kinetics of migration and diffusion of Mg cation ions. The decomposition of the electrolyte is happening in the voltage above ~0.4 V in fresh Mg sample and its repeated reaction is observed. Galvanostatic charge–discharge profiles of the 1st and 2nd cycle for (c) fresh Mg and (d) MgF_2@Mg foil at a current density of 30 mA g^{-1}. The electrochemical measurements were carried out at 25 °C in 2025 coin cells. Capacity is calculated based on the weight of the active material mass of Bi.

cell with fresh Mg decreased from 416 to 275 mAh g^{-1} with over 100% of Coulombic efficiency in the first seven cycles, then the capacity gradually increased in the subsequent cycle. This can be ascribed to the activation process identified from the CV results. More importantly, the APC electrolyte fails to form a stable passivating layer on Mg, which continually consumes the electrolyte during cycling and leads to the increased irreversible capacity. Note that the Coulombic efficiency also fluctuates during cycling and the charge capacity remains 232 mAh g^{-1} after 50 cycles. This can be ascribed to the compacted Bi nanorods in the present work that might suffer from serious structural transformation resulted from the large volume change (~100%) during the alloying and de-alloying process. It might contribute to the capacity fading with a loss of electrical contact between the active material and the conductive additive. More importantly, the voltage profiles of the fresh Mg electrode between 0.01 and 1 V with representative cycles reveal that the voltage of the discharge plateau is decreased, while the charging voltage increases during cycling, as shown in Fig. 4b. It indicates the polarization of the electrodes increase because of the slow kinetics and reduced Mg^{2+} diffusion/migration in the charge/discharge process after long cycling. These results suggest that the surface film formed in fresh Mg is unstable and the film seems to be electronically conductive because side reactions at Mg continue throughout testing, and results in the formation of a passivating layer which causes the fast deterioration of the cells in the long cycling. However, for Mg coated with MgF_2, the charge capacity is 342 mAh g^{-1} at the current density of 30 mA g^{-1} and the capacity remains 286 mAh g^{-1} after 50 cycles, exhibiting better capacity retention compared to fresh Mg. The Coulombic efficiency after the second cycle is nearly 100% during all subsequent cycles. Remarkably, no obvious change in galvanostatic voltage profiles during the long-term cycling (Fig. 4c), demonstrating the decent stability of the surface film after the MgF_2 coating. It is believed that the passivating layer formed by MgF_2 suppresses the electrolyte decomposition and eliminates the side reactions between Mg and the APC electrolyte leading to lower polarization and improved cycling stability.

The rate performance of the cell with fresh Mg or with MgF_2@Mg at various charge-discharge current densities were evaluated and compared. The cells were tested at 30, 120, 300, 600, 1800, and 3000 mA g^{-1} in turn as shown in Fig. 4d, the corresponding discharge capacities are 307, 280, 275, 272, 184, and 152 mAh g^{-1} for Mg and 317, 322, 321, 329, 227, and 226 mAh g^{-1} for MgF_2@Mg, respectively. The MgF_2@Mg electrode also displays a good capacity recovery when the current density switches back from 3000 mA g^{-1} to 30 mA g^{-1}, suggesting good electrode structure stability and reaction reversibility. This enhanced rate performance is attributed to the good ionic conductivity through MgF_2 buffer layer and the suppressed side reaction and the favourable interfacial properties between the electrodes and the electrolyte in the cell.

In order to further confirm the Mg^{2+} conduction behavior, electrochemical impedance spectroscopy (EIS) tests were also carried out at room temperature. Fig. 4e shows the comparative impedance Nyquist plots for the cells consisting of fresh Mg and MgF_2@Mg electrode after 3 cycles. The experiments results show depressed semi-circle response for both of the electrodes, suggesting porosity within the electrode surface [61]. Fitting the Nyquist plots with an equivalent circuit (inset) composed of internal resistance (R_s), passivation film resistance (R_f), and charge transfer resistance (R_{ct}). After coating with MgF_2, the overall resistance ($R_s + R_f + R_{ct}$) is smaller than that of fresh Mg foil, as shown in Table 1. This result indicates that the MgF_2 layer is ionic conductive, which ensuring Mg^{2+} transport and preventing the electrolyte decomposition while accommodating the reversible Mg deposition/stripping process.

The surface morphology of the Mg foils before cycling and the Mg electrodes taken from the cell after three cycles were observed by SEM, as shown in Fig. 5. Each image includes an inset that shows the electrode's appearance. The relevant EDS spectrum is also presented at the bottom of each image and the elemental content estimated from EDS is shown in Table 2. Prior to cycling, the surface of the fresh Mg foil is smooth with a metallic color and some wrinkle-like features in the SEM, as shown in Fig. 5a, which resulted from the HCl washing process. The existence of carbon and oxygen in Fig. 5e are attributed to the carbonate and oxidation or the adsorption of the CO_2 and O_2 when the samples were exposed to the air while the sample was transferred. A sharp magnesium peak can be observed and chlorine is excluded in the as-prepared fresh Mg foil. This confirms that HCl is removed completely after the washing process. After soaking in HF, the Mg foil becomes slightly yellow and a layer of deposit with nanoparticles between 10 and 20 nm in size was stacked on the Mg, as shown in Fig. 5c. This feature can produce a flexible and ionic conductive framework with a porous structure at the surface, likely formed by H_2 gas bubbles during the HF treatment and supported by BET data (Fig. S1). At the metal-MgF_2 interface, the conformal coating allows for the insertion/extraction of Mg-ions, which is confirmed by the CV results in Fig. 3a and b. The EDS result shows that the deposit is rich in fluorine (Fig. 5g). Meanwhile, the uniform distribution of MgF_2 in the composite is verified by EDS element mapping analysis (Fig. S3b). These results indicate the MgF_2 successfully coated the entire surface of the Mg foil. It is believed that the conformal surface layer at the metal-MgF_2 interface suppresses electrolyte decomposition while the porous structure at the electrolyte-MgF_2 enhances the area available for the reversible reaction: $Mg^{2+} + 2e^- \leftrightarrow Mg$. When the cell with fresh Mg was charged and discharged three times, a rougher Mg surface was observed to turn dark and a thick fluffy deposit was padded on the Mg, as shown in Fig. 5b. Corresponding EDS of cycled Mg foil is illustrated in Fig. 5f. The spectrum of uncoated Mg foil shows significantly higher peaks for aluminum and chlorine at 1.5 keV and 2.6 keV, respectively, and the carbon and oxygen content increased compared to the pre-cycled Mg foil (Table 2). Since aluminum and chlorine exist only in APC electrolyte, but not in Mg foil or in Bi electrode, it clearly proves that the thick layer is derived from insoluble precipitates from the APC electrolyte [6,59]. However, this situation did not happen when Mg was coated with the MgF_2 passivating layer. After three cycles, only slight visual changes to the Mg electrode surface are observed and compact nanoparticles can be clearly resolved (Fig. 5d). The elemental analysis shows that carbon and oxygen on the surface increase only slightly after cycling (Table 2), and their uniform deposition on the Mg surface was clearly identified via the elemental mapping image (Fig. S3d). It confirms that the passivating layer formed by MgF_2 acts as a physical barrier that suppresses the chemical reaction between the Mg foil and the APC electrolyte but simultaneously supports Mg-ion transport, as demonstrated in Fig. 1b.

The discovery of Mg^{2+}-conducting surface films contradicts conventional wisdom that passivation films on Mg metal are fully insulating [7] and the assumption that MgF_2 would be impassable to Mg^{2+} [8,62]. However, this discrepancy can be resolved with a close reading of the literature. Lu et al.'s original study [7] and recent results from Aurbach's lab [8] show that electrolytes using PF_6^- will passivate Mg anodes. However, the conformal MgF_2 surface film formed from our treatment likely bears little resemblance to the fluoride-containing surface film formed when PF_6^- anions or solvent molecules are reduced at the metal surface. The nature of the MgF_2 film and the reasons behind why it permits Mg^{2+} transport deserve further study so that improved Mg-conducting SEI layers or solid-state electrolytes might be developed.

Overall, the Mg electrodes coated with MgF_2 perform better than those based on fresh Mg foil. By carefully studying the morphology and the structure-property relationship, we propose the following main reasons for the high performance. First, the MgF_2 coating help protect the APC electrolyte from decomposition on Mg surface. The stable passivating layer prevents the direct exposure of magnesium to the APC electrolyte and, thus, enhance the stability of electrolyte (as shown in Fig. 1). This is supported by the fact that the major difference in irreversible capacity comes from the first and second charge curve. Second, it is possible the MgF_2 benefits the electrochemical performance, since MgF_2 has been reported to facilitate Mg^{2+} conductivity in the electrolyte as salt [63,64]. In addition, the MgF_2 layer not only suppresses further

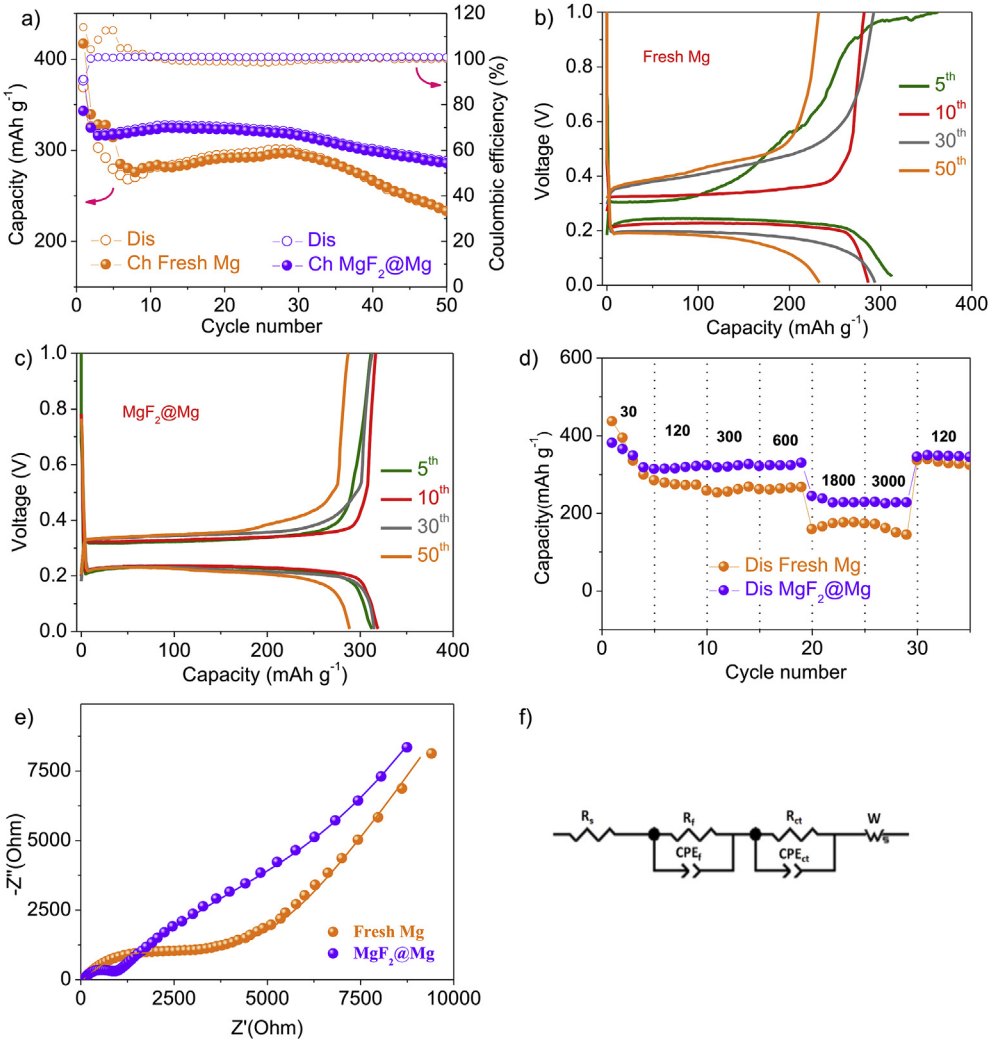

Fig. 4. Charge-discharge tests using Bi nanorods as positive electrode and different magnesium foils as negative electrodes: (a) Cycling performance of fresh Mg and MgF_2@Mg foil in the range of 0.01-1.0 V, charge-discharge voltage profiles of fresh Mg (b) and MgF_2@Mg (c) at a current density of 120 mA g^{-1} between 0.01 and 1.0 V. (d) The comparison of the rate capability of the fresh Mg and MgF_2@Mg at different current densities. The cells were tested at 30 mA g^{-1}, 120 mA g^{-1}, 300 mA g^{-1}, 600 mA g^{-1}, 1800 mA g^{-1}, and 3000 mA g^{-1}. (e) Electrochemical impedance spectroscopy and fitting results for fresh Mg and MgF_2@Mg foil after 3 cycles. (f) Equivalent electrical circuit model for the EIS.

electrolyte decomposition but also increases Mg^{2+} transport at the interface between Mg foil and electrolyte because the intercalation/deintercalation reaction occurs on a large surface area. Finally, the passivating MgF_2 layer is carefully designed so that the passivating layer covers almost all the exposed surface of Mg, which minimizes the side chemical reaction and helps improve interfacial compatibility between electrode and APC electrolyte.

3. Conclusions

Improved compatibility between Mg metal and the electrolyte interface can be achieved by inserting an ionically conductive but electronically insulating magnesium fluoride (MgF_2) layer, which can be formed by simply immersing Mg in hydrofluoric acid. With this passivating layer, the voltage stability, Coulombic efficiency and cycling performance of a bismuth (Bi)/magnesium (Mg) cell are appreciably improved. This is attributed to successful suppression of the electrolyte side reactions. To the best of our knowledge, this is the first Mg^{2+}-conducting SEI layer ever reported, and this design principle for Mg metal surface chemistry has important applications in Mg ion battery storage technology.

Table 1
Fitting results of EIS for fresh Mg and MgF_2@Mg foil.

Sample	R_s (Ω)	R_f (Ω)	R_{ct} (Ω)
Fresh Mg	60	2553	4800
MgF_2@Mg	114	1022	5331

4. Methods

Preparation of MgF_2 modified Mg foil. To prepare fresh Mg foil, the commercial Mg foils were immersed into 0.1 M HCl solution for 2 min until the oxidation layer was removed and washed with THF several times and then dried in vacuum oven at room temperature. Then the Mg foils were transferred into glovebox and mechanically polished with sand paper (2000 grit) and wiped with THF prior to use. MgF_2 modified Mg foil were prepared by reacting HF and fresh metallic Mg as follows. The fresh Mg foils were immersed into 0.2 M hydrofluoric acid solution and sonicated for 5 min at room temperature to obtain the MgF_2 layer. Then, the Mg foils were washed with THF and dried in a vacuum oven at room temperature and transferred into the glovebox.

Synthesis of Bi nanorods cathode. The Bi cathode materials were synthesized using a solvothermal method according to the reported procedure previously [57]. In a typical procedure, 0.466 g Bi_2O_3 was added to 30 ml pure ethylene glycol (EG) whilst stirring with a magnetic stirrer for 30 min at room temperature. The mixture was then transferred into a stainless-steel autoclave with a Teflon liner and kept at 200 °C for 12 h. The black precipitate was collected and washed several times by centrifugation with diluted hydrochloric acid and deionized water after the autoclave was cooled down, and then dried at 80 °C overnight.

Materials characterization. The crystal structure of the composite was determined by XRD (D8 Bruker X-ray diffractometer with Cu-Kα

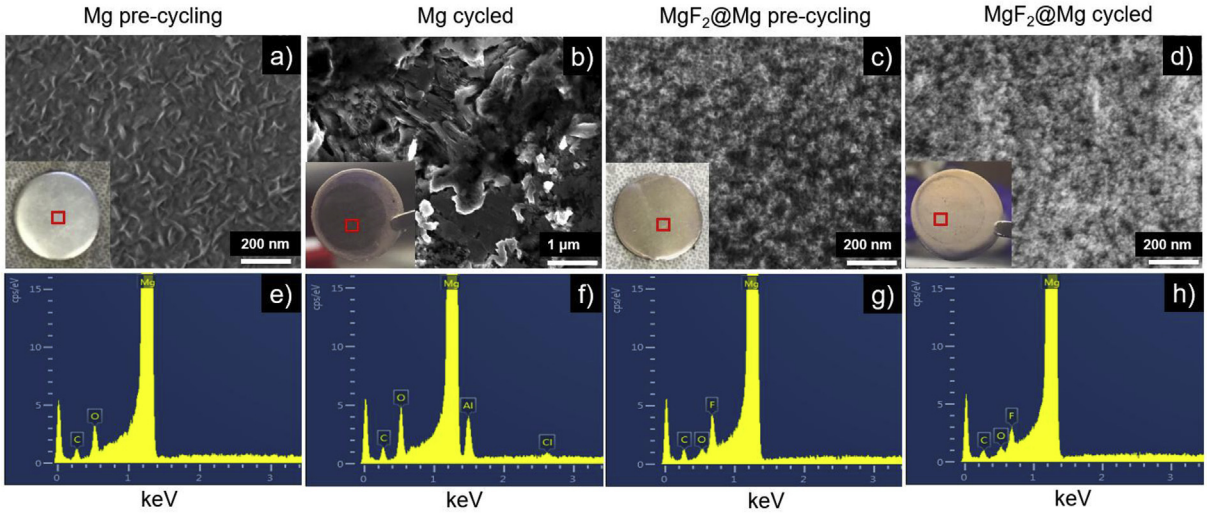

Fig. 5. SEM images of Mg electrodes: fresh Mg before cycling (a) and fresh Mg after 3 cycles (b), MgF_2@Mg before cycling (c) and MgF_2@Mg after 3 cycles (d). Photographs of the Mg electrodes disassembled from coin cells are shown in the inset. In the fresh sample with MgF_2 coating, the Mg surface was covered by a nanoparticles sized layer, which is able to prevent the electrolyte decomposition. EDS patterns of the surface of the Mg electrodes: fresh Mg before cycling (e) and fresh Mg after 3 cycles (f), MgF_2@Mg before cycling (g) and MgF_2@Mg after 3 cycles (h).

Table 2
Element contents of the samples from the EDS.

Sample	Mg (%)	O (%)	C (%)	F (%)	Al (%)	Cl (%)
Mg pre-cycling	91.9	2.4	5.7	–	–	–
Mg after cycling	85.4	4.3	7.3	–	2.8	0.2
MgF_2@Mg pre-cycling	92.1	0.6	5.5	1.8	–	–
MgF_2@Mg after cycling	92.5	0.9	5.6	1.0	–	–

radiation ($\lambda = 1.5418$ Å)) within the range of 10°–80° (2θ). The morphology was observed by TEM (JEOL JEM-2100HR) and SEM (JEOL JSM-7000F), and the element contents were analyzed with EDS on the JEOL JSM-7000F SEM. The specific surface area and pore characteristics were determined by multipoint BET and BJH desorption analyses, respectively.

Electrochemical measurements. The Bi electrode was prepared by coating a mixture of 70 wt. % active material and 15 wt. % Super-P as conducting agent and 15 wt. % polyvinylidene fluoride (PVdF) as binder onto an Al current collector. 2025-type coin cells were assembled in an Ar-filled MBraun glove box (water and oxygen contents were lower than 0.1 ppm) using the prepared Bi electrodes as positive electrodes, Mg foils as negative electrodes and microporous membrane (Celgard 2400) as the separators. The APC electrolyte comprised of PhMgCl and $AlCl_3$ in a ratio of 2:1 was used in this study has been reported in previous literature [32]. In brief, 10 ml of 0.5 M $AlCl_3$-THF solution (Sigma-Aldrich) was added drop by drop in 10 ml of 1 M PhMgCl-THF solution, then stirred at least 24 h prior to use. For the galvanostatic cycling test in symmetrical cells, the cells were cycled at 0.25 mA cm^{-2} for 1 h in each half cycle. In the battery assembly, fresh Mg-metal electrode or MgF_2@Mg-metal electrode was used as the working electrode and the counter electrode, and APC was used as the electrolyte. CV was performed on Solartron-1470 instrument (England) with Bi as the positive electrode and Mg as the negative electrode at 25 °C at a sweep rate of 0.1 mV s^{-1}. The charge-discharge tests were conducted on a LAND cell test system (Land CT 2001A) and cycled between 1.0 V and 0.01 V at 25 °C, and the capacity of the cells were calculated based on the mass of the active material.

Acknowledgements

This work was supported by the National Science Foundation (CBET-1803256), and China Postdoctoral Science Foundation (Grant Nos. 2017M622625). Part of this work was conducted at the Molecular Analysis Facility, a National Nanotechnology Coordinated Infrastructure site at the University of Washington which is supported in part by the National Science Foundation (grant NNCI-1542101), the University of Washington, the Molecular Engineering & Sciences Institute, and the Clean Energy Institute.

Appendix A. Supplementary data

Supplementary data to this article can be found online at https://doi.org/10.1016/j.ensm.2019.06.035.

References

[1] D. Aurbach, Z. Lu, A. Schechter, Y. Gofer, H. Gizbar, R. Turgeman, Y. Cohen, M. Moshkovich, E. Levi, Prototype systems for rechargeable magnesium batteries, Nature 407 (2000) 724–727, https://doi.org/10.1038/35037553.
[2] Y. Cheng, Y. Shao, L.R. Parent, M.L. Sushko, G. Li, P.V. Sushko, N.D. Browning, C. Wang, J. Liu, Interface promoted reversible Mg insertion in nanostructured Tin-antimony alloys, Adv. Mater. 27 (2015) 6598–6605, https://doi.org/10.1002/adma.201502378.
[3] H.D. Yoo, I. Shterenberg, Y. Gofer, G. Gershinsky, N. Pour, D. Aurbach, Mg rechargeable batteries: an on-going challenge, Energy Environ. Sci. 6 (2013) 2265–2279, https://doi.org/10.1039/c3ee40871j.
[4] R.C. Massé, E. Uchaker, G. Cao, Beyond Li-ion: electrode materials for sodium- and magnesium-ion batteries, China Mater 58 (2015) 715–766, https://doi.org/10.1007/s40843-015-0084-8.
[5] J. Muldoon, C.B. Bucur, A.G. Oliver, T. Sugimoto, M. Matsui, H.S. Kim, G.D. Allred, J. Zajicek, Y. Kotani, Electrolyte roadblocks to a magnesium rechargeable battery, Energy Environ. Sci. 5 (2012) 5941–5950, https://doi.org/10.1039/c2ee03029b.
[6] R.E. Doe, R. Han, J. Hwang, A.J. Gmitter, I. Shterenberg, H.D. Yoo, N. Pourb, D. Aurbach, Novel, electrolyte solutions comprising fully inorganic salts with high anodic stability for rechargeable magnesium batteries, Chem. Commun. (Camb) 50 (2014) 243–245, https://doi.org/10.1039/c3cc47896c.
[7] Z. Lu, A. Schechter, M. Moshkovich, D. Aurbach, On the electrochemical behavior of magnesium electrodes in polar aprotic electrolyte solutions, J. Electroanal. Chem. 466 (1999) 203–217, https://doi.org/10.1016/S0022-0728(99)00146-1.
[8] I. Shterenberg, M. Salama, Y. Gofer, D. Aurbach, Hexafluorophosphate-based solutions for Mg batteries and the importance of chlorides, Langmuir 33 (2017) 9472–9478, https://doi.org/10.1021/acs.langmuir.7b01609.
[9] Y. Cheng, R.M. Stolley, K.S. Han, Y. Shao, B. Arey, N. Washton, K.T. Mueller, M.L. Helm, V.L. Sprenkle, J. Liu, G. Li, Highly active electrolytes for rechargeable Mg batteries based on $[Mg_2(\mu\text{-}Cl)_2]^{2+}$ cation complex in dimethoxyethane, Phys. Chem. Chem. Phys. 17 (2015) 13307–13314, https://doi.org/10.1039/C5CP00859J.
[10] H.S. Kim, T.S. Arthur, G.D. Allred, J. Zajicek, J.G. Newman, A.E. Rodnyansky, A.G. Oliver, W.C. Boggess, J. Muldoon, Structure and compatibility of a magnesium electrolyte with a sulphur cathode, Nat. Commun. 2 (2011) 427, https://doi.org/10.1038/ncomms1435.

[11] C. Liebenow, Z. Yang, P. Lobitz, The electrodeposition of magnesium using solutions of organomagnesium halides, amidomagnesium halides and magnesium organoborates, Electrochem. Commun. 2 (2000) 641–645, https://doi.org/10.1016/S1388-2481(00)00094-1.

[12] D. Aurbach, H. Gizbar, A. Schechter, O. Chusid, H.E. Gottlieb, Y. Gofer, I. Goldberg, Electrolyte solutions for rechargeable magnesium batteries based on organomagnesium chloroaluminate complexes, J. Electrochem. Soc. 149 (2002) A115–A121, https://doi.org/10.1149/1.1429925.

[13] Y. Gofer, O. Chusid, H. Gizbar, Y. Viestfrid, H.E. Gottlieb, V. Marks, D. Aurbach, Improved electrolyte solutions for rechargeable magnesium batteries, Electrochem. Electrochem. Solid-State Lett. 9 (2006) A257–A260, https://doi.org/10.1149/1.2186003.

[14] N. Pour, Y. Gofer, D.T. Major, D. Aurbach, Structural analysis of electrolyte solutions for rechargeable Mg batteries by stereoscopic means and DFT calculations, J. Am. Chem. Soc. 133 (2011) 6270–6278, https://doi.org/10.1021/ja1098512.

[15] C.B. Bucur, T. Gregory, J. Muldoon, Why Grignard's Century Old Nobel Prize Should Spark Your Curiosity, 2015, pp. 611–635, https://doi.org/10.1007/978-3-319-15458-9_22.

[16] J. Muldoon, C.B. Bucur, T. Gregory, Fervent hype behind magnesium batteries: an open call to synthetic chemists - electrolytes and cathodes needed, Angew. Chem. Int. Ed. 56 (2017) 12064–12084, https://doi.org/10.1002/anie.201700673.

[17] O. Tutusaus, R. Mohtadi, T.S. Arthur, F. Mizuno, E.G. Nelson, Y.V. Sevryugina, An efficient halogen-free electrolyte for use in rechargeable magnesium batteries, Angew. Chem. Int. Ed. (2015) 7900–7904, https://doi.org/10.1002/anie.201412202, 201412202.

[18] E.G. Nelson, J.W. Kampf, B.M. Bartlett, Enhanced oxidative stability of non-Grignard magnesium electrolytes through ligand modification, Chem. Commun. (Camb) 50 (2014) 5193–5195, https://doi.org/10.1039/c3cc47277a.

[19] J.L. Esbenshade, C.J. Barile, T.T. Fister, K.L. Bassett, P. Fenter, R.G. Nuzzo, A.A. Gewirth, Improving electrodeposition of Mg through an open circuit potential hold, J. Phys. Chem. C 119 (2015) 23366–23372, https://doi.org/10.1021/acs.jpcc.5b07825.

[20] K.A. See, K.W. Chapman, L. Zhu, K.M. Wiaderek, O.J. Borkiewicz, C.J. Barile, P.J. Chupas, A.A. Gewirth, The interplay of Al and Mg speciation in advanced Mg battery electrolyte solutions, J. Am. Chem. Soc. 138 (2016) 328–337, https://doi.org/10.1021/jacs.5b10987.

[21] O. Tutusaus, R. Mohtadi, N. Singh, T.S. Arthur, F. Mizuno, Study of electrochemical phenomena observed at the Mg metal/electrolyte interface, ACS Energy Lett. 2 (2016) 224–229, https://doi.org/10.1021/acsenergylett.6b00549.

[22] S.-B. Son, T. Gao, S.P. Harvey, K.X. Steirer, A. Stokes, A. Norman, C. Wang, A. Cresce, K. Xu, C. Ban, An artificial interphase enables reversible magnesium chemistry in carbonate electrolytes, Nat. Chem. 10 (2018) 532–539, https://doi.org/10.1038/s41557-018-0019-6.

[23] X. Li, T. Gao, F. Han, Z. Ma, X. Fan, S. Hou, N. Eidson, W. Li, C. Wang, Reducing Mg anode overpotential via ion conductive surface layer formation by iodine additive, Adv. Energy Mater. (2017) 1–6, https://doi.org/10.1002/aenm.201701728, 1701728.

[24] R. Attias, M. Salama, B. Hirsch, Y. Goffer, D. Aurbach, Anode-electrolyte interfaces in secondary magnesium batteries, Joule 3 (2018) 1–26, https://doi.org/10.1016/j.joule.2018.10.028.

[25] Y. Gofer, R. Turgeman, H. Cohen, D. Aurbach, XPS investigation of surface chemistry of magnesium electrodes in contact with organic solutions of organochloroaluminate complex salts, Langmuir 19 (2003) 2344–2348, https://doi.org/10.1021/la026642c.

[26] P. Canepa, G.S. Gautam, R. Malik, S. Jayaraman, Z. Rong, K.R. Zavadil, K. Persson, G. Ceder, Understanding the initial stages of reversible Mg deposition and stripping in inorganic non-aqueous electrolytes, Chem. Mater. 27 (2015) 3317–3325, https://doi.org/10.1021/acs.chemmater.5b00389.

[27] J.G. Connell, B. Genorio, P.P. Lopes, D. Strmcnik, V.R. Stamenkovic, N.M. Markovic, Tuning the reversibility of Mg anodes via controlled surface passivation by H_2O/Cl^- in organic electrolytes, Chem. Mater. 28 (2016) 8268–8277, https://doi.org/10.1021/acs.chemmater.6b03227.

[28] B. Pan, J. Huang, N. Sa, S.M. Brombosz, J.T. Vaughey, L. Zhang, A.K. Burrell, Z. Zhang, C. Liao, $MgCl_2$: the key ingredient to improve chloride containing electrolytes for rechargeable magnesium-ion batteries, J. Electrochem. Soc. 163 (2016) A1672–A1677, https://doi.org/10.1149/2.0821608jes.

[29] J. Muldoon, C.B. Bucur, A.G. Oliver, J. Zajicek, G.D. Allred, W.C. Boggess, Corrosion of magnesium electrolytes: chlorides – the culprit, Energy Environ. Sci. 6 (2013) 482–487, https://doi.org/10.1039/c2ee23686a.

[30] D. Lv, T. Xu, P. Saha, M.K. Datta, M.L. Gordin, A. Manivannan, P.N. Kumta, D. Wang, A scientific study of current collectors for Mg batteries in $Mg(AlCl_2EtBu)_2$/THF electrolyte, J. Electrochem. Soc. 160 (2012) A351–A355, https://doi.org/10.1149/2.085302jes.

[31] O. Tutusaus, R. Mohtadi, Paving the way towards highly stable and practical electrolytes for rechargeable magnesium batteries, ChemElectroChem 2 (2015) 51–57, https://doi.org/10.1002/celc.201402207.

[32] O. Mizrahi, N. Amir, E. Pollak, O. Chusid, V. Marks, H. Gottlieb, L. Larush, E. Zinigrad, D. Aurbach, Electrolyte solutions with a wide electrochemical window for rechargeable magnesium batteries, J. Electrochem. Soc. 155 (2008) A103–A109, https://doi.org/10.1149/1.2806175.

[33] Y. Guo, F. Zhang, J. Yang, F. Wang, Y. NuLi, S. Hirano, Boron-based electrolyte solutions with wide electrochemical windows for rechargeable magnesium batteries, Energy Environ. Sci. 5 (2012) 9100–9106, https://doi.org/10.1039/c2ee22509c.

[34] E.G. Nelson, S.I. Brody, J.W. Kampf, B.M. Bartlett, A magnesium tetraphenylaluminate battery electrolyte exhibits a wide electrochemical potential window and reduces stainless steel corrosion, J. Mater. Chem. 2 (2014) 18194–18198, https://doi.org/10.1039/C4TA04625K.

[35] C.B. Bucur, T. Gregory, A.G. Oliver, J. Muldoon, Confession of a magnesium battery, J. Phys. Chem. Lett. 6 (2015) 3578–3591, https://doi.org/10.1021/acs.jpclett.5b01219.

[36] K. Xu, A. von Cresce, Interfacing electrolytes with electrodes in Li ion batteries, J. Mater. Chem. 21 (2011) 9849–9864, https://doi.org/10.1039/c0jm04309e.

[37] B. Li, M. Xu, T. Li, W. Li, S. Hu, Prop-1-ene-1,3-sultone as SEI formation additive in propylene carbonate-based electrolyte for lithium ion batteries, Electrochem. Commun. 17 (2012) 92–95, https://doi.org/10.1016/j.elecom.2012.02.016.

[38] B. Li, Y. Wang, H. Rong, Y. Wang, J. Liu, L. Xing, M. Xu, W. Li, A novel electrolyte with the ability to form a solid electrolyte interface on the anode and cathode of a $LiMn_2O_4$/graphite battery, J. Mater. Chem. 1 (2013) 12954–12961, https://doi.org/10.1039/c3ta13067c.

[39] S. Jeong, M. Inaba, R. Mogi, Y. Iriyama, T. Abe, Z. Ogumi, Surface film formation on a graphite negative electrode in lithium-ion batteries: atomic force microscopy study on the effects of film-forming additives in propylene carbonate, Langmuir 27 (2001) 8281–8286. http://pubs.acs.org/doi/abs/10.1021/la015553h.

[40] D. Aurbach, K. Gamolsky, B. Markovsky, Y. Gofer, M. Schmidt, U. Heider, On the use of vinylene carbonate (VC) as an additive to electrolyte solutions for Li-ion batteries, Electrochim. Acta 47 (2002) 1423–1439, https://doi.org/10.1016/S0013-4686(01)00858-1.

[41] M.-H. Ryou, G.-B. Han, Y.M. Lee, J.-N. Lee, D.J. Lee, Y.O. Yoon, J.-K. Park, Effect of fluoroethylene carbonate on high temperature capacity retention of $LiMn_2O_4$/graphite Li-ion cells, Electrochim. Acta 55 (2010) 2073–2077, https://doi.org/10.1016/j.electacta.2009.11.036.

[42] B. Li, Y. Wang, H. Lin, J. Liu, L. Xing, M. Xu, W. Li, Improving high voltage stability of lithium cobalt oxide/graphite battery via forming protective films simultaneously on anode and cathode by using electrolyte additive, Electrochim. Acta 141 (2014) 263–270, https://doi.org/10.1016/j.electacta.2014.07.085.

[43] M. Xu, W. Li, B.L. Lucht, Effect of propane sultone on elevated temperature performance of anode and cathode materials in lithium-ion batteries, J. Power Sources 193 (2009) 804–809, https://doi.org/10.1016/j.jpowsour.2009.03.067.

[44] B. Li, M. Xu, B. Li, Y. Liu, L. Yang, W. Li, S. Hu, Properties of solid electrolyte interphase formed by prop-1-ene-1,3-sultone on graphite anode of Li-ion batteries, Electrochim. Acta 105 (2013) 1–6, https://doi.org/10.1016/j.electacta.2013.04.142.

[45] H. Lee, S. Kim, Y. Park, Enhanced electrochemical properties of fluoride-coated $LiCoO_2$ thin films, Nanoscale Res. Lett. 7 (2012) 16, https://doi.org/10.1186/1556-276X-7-16.

[46] J. Zhao, L. Liao, F. Shi, T. Lei, G. Chen, A. Pei, J. Sun, K. Yan, G. Zhou, J. Xie, C. Liu, Y. Li, Z. Liang, Z. Bao, Y. Cui, Surface fluorination of reactive battery anode materials for enhanced stability, J. Am. Chem. Soc. 139 (2017) 11550–11558, https://doi.org/10.1021/jacs.7b05251.

[47] J. Lang, Y. Long, J. Qu, X. Luo, H. Wei, K. Huang, H. Zhang, L. Qi, Q. Zhang, Z. Li, H. Wu, One-pot solution coating of high quality LiF layer to stabilize Li metal anode, Energy Storage Mater. 16 (2019) 85–90, https://doi.org/10.1016/j.ensm.2018.04.024.

[48] L. Suo, O. Borodin, T. Gao, M. Olguin, J. Ho, X. Fan, C. Luo, C. Wang, K. Xu, Water-in-salt" electrolyte enables high-voltage aqueous lithium-ion chemistries, Science 350 (2015) 938–943, https://doi.org/10.1126/science.aab1595.

[49] Q. Zhang, J. Pan, P. Lu, Z. Liu, M.W. Verbrugge, B.W. Sheldon, Y.-T. Cheng, Y. Qi, X. Xiao, Synergetic effects of inorganic components in solid electrolyte interphase on high cycle efficiency of lithium ion batteries, Nano Lett. 16 (2016) 2011–2016, https://doi.org/10.1021/acs.nanolett.5b05283.

[50] Y. Bai, K. Jiang, S. Sun, Q. Wu, X. Lu, N. Wan, Performance improvement of $LiCoO_2$ by MgF_2 surface modification and mechanism exploration, Electrochim. Acta 134 (2014) 347–354, https://doi.org/10.1016/j.electacta.2014.04.155.

[51] Y. Cho, J. Eom, J. Cho, High performance $LiCoO_2$ cathode materials at 60°C for lithium secondary batteries prepared by the facile nanoscale dry-coating method, J. Electrochem. Soc. 157 (2010) A617–A624, https://doi.org/10.1149/1.3332676.

[52] H.J. Lee, Y.J. Park, Interface characterization of MgF_2-coated $LiCoO_2$ thin films, Solid State Ionics 230 (2013) 86–91, https://doi.org/10.1016/j.ssi.2012.08.003.

[53] A.B.D. Nandiyanto, F. Iskandar, T. Ogi, K. Okuyama, Nanometer to submicrometer magnesium fluoride particles with controllable morphology, Langmuir 26 (2010) 12260–12266, https://doi.org/10.1021/la101194w.

[54] D. Aurbach, G.S. Suresh, E. Levi, A. Mitelman, O. Mizrahi, O. Chusid, M. Brunelli, Progress in rechargeable magnesium battery technology, Adv. Mater. 19 (2007) 4260–4267, https://doi.org/10.1002/adma.200701495.

[55] T.S. Arthur, N. Singh, M. Matsui, Electrodeposited Bi, Sb and $Bi_{1-x}Sb_x$ alloys as anodes for Mg-ion batteries, Electrochem. Commun. 16 (2012) 103–105, https://doi.org/10.1016/j.elecom.2011.12.010.

[56] Y. Shao, M. Gu, X. Li, Z. Nie, P. Zuo, G. Li, T. Liu, J. Xiao, Y. Cheng, C. Wang, J.-G. Zhang, J. Liu, Highly reversible Mg insertion in nanostructured Bi for Mg ion batteries, Nano Lett. 14 (2013) 255–260, https://doi.org/10.1021/nl403874y.

[57] X. Liu, J. Zeng, S. Zhang, R. Zheng, X. Liu, Y. Qian, Novel bismuth nanotube arrays synthesized by solvothermal method, Chem. Phys. Lett. 374 (2003) 348–352, https://doi.org/10.1016/S0009-2614(03)00730-9.

[58] M.M. Huie, D.C. Bock, E.S. Takeuchi, A.C. Marschilok, K.J. Takeuchi, Cathode materials for magnesium and magnesium-ion based batteries, Coord. Chem. Rev. 287 (2015) 15–27, https://doi.org/10.1016/j.ccr.2014.11.005.

[59] F. Murgia, L. Stievano, L. Monconduit, R. Berthelot, Insight into the electrochemical behavior of micrometric Bi and Mg_3Bi_2 as high performance negative electrodes for Mg batteries, J. Mater. Chem. 3 (2015) 16478–16485, https://doi.org/10.1039/C5TA04077A.

[60] D.S. Tchitchekova, D. Monti, P. Johansson, F. Bardé, A. Randon-Vitanova, M.R. Palacín, A. Ponrouch, On the reliability of half-cell tests for monovalent (Li^+, Na^+) and divalent (Mg^{2+}, Ca^{2+}) cation based batteries, J. Electrochem. Soc. 164 (2017) A1384–A1392, https://doi.org/10.1149/2.0411707jes.
[61] V.F. Lvovich, Impedance Spectroscopy Applications to Electrochemical and Dielectric Phenomena, Wiley, New Jersey, 2012.
[62] E.N. Keyzer, H.F.J. Glass, Z. Liu, P.M. Bayley, S.E. Dutton, C.P. Grey, D.S. Wright, $Mg(PF_6)_2$-Based electrolyte systems: understanding electrolyte-electrode interactions for the development of Mg-ion batteries, J. Am. Chem. Soc. 138 (2016) 8682–8685, https://doi.org/10.1021/jacs.6b04319.
[63] B. Børresen, G.M. Haarberg, R. Tunold, Electrodeposition of magnesium from halide melts—charge transfer and diffusion kinetics, Electrochim. Acta 42 (1997) 1613–1622, https://doi.org/10.1016/S0013-4686(96)00322-2.
[64] Z. Zhang, Z. Cui, L. Qiao, J. Guan, H. Xu, X. Wang, P. Hu, H. Du, S. Li, X. Zhou, S. Dong, Z. Liu, G.L. Cui, Novel design concepts of efficient Mg-ion electrolytes toward high-performance magnesium-selenium and magnesium-sulfur batteries, Chen, Adv. Energy Mater. 201602055 (2017) 1–10, https://doi.org/10.1002/aenm.201602055.